

The role of conductivity discontinuities in design of cardiac defibrillation

Hyunkyung Lim,¹ Wenjing Cun,¹ Yue Wang,¹ Richard A. Gray,² and James Glimm¹

¹*Department of Applied Mathematics and Statistics, Stony Brook University,
Stony Brook, NY 11794-3600, USA*

²*Center for Devices and Radiological Health, Food and Drug Administration,
Silver Spring, MD 20993-0002, USA*

Fibrillation is an erratic electrical state of the heart, of rapid twitching rather than organized contractions. Ventricular fibrillation is fatal if not treated promptly. The standard treatment, defibrillation, is a strong electrical shock to reinitialize the electrical dynamics and allow a normal heart beat. Both the normal and the fibrillatory electrical dynamics of the heart are organized into moving wave fronts of changing electrical signals, especially in the transmembrane voltage, which is the potential difference between the cardiac cellular interior and the intracellular region of the heart. In a normal heart beat, the wave front motion is from bottom to top and is accompanied by the release of Ca ions to induce contractions and pump the blood. In a fibrillatory state, these wave fronts are organized into rotating scroll waves, with a centerline known as a filament. Treatment requires altering the electrical state of the heart through an externally applied electrical shock, in a manner that precludes the existence of the filaments and scroll waves. Detailed mechanisms for the success of this treatment are partially understood, and involve local shock-induced changes in the transmembrane potential, known as virtual electrode alterations. These transmembrane alterations are located at boundaries of the cardiac tissue, including blood vessels and the heart chamber wall, where discontinuities in electrical conductivity occur. The primary focus of this paper is the defibrillation shock and the subsequent electrical phenomena it induces. Six partially overlapping causal factors for defibrillation success are identified from the literature. We present evidence in favor of five of these and against one of them. A major conclusion is that a dynamically growing wave front, starting at the heart surface appears to play a primary role during defibrillation by critically reducing the volume required to sustain the dynamic motion of scroll waves; in contrast, virtual electrode occurring at boundaries of small, isolated blood vessels only cause minor effects. As a consequence, we suggest that the size of the heart (specifically, the surface to volume ratio) is an important defibrillation variable.

Fibrillation is an erratic state of the electrical signals in the heart, characterized by twitching rather than organized contractions. It is fatal if not treated promptly. It is a common cause of cardiac arrest, with 350,000 out of hospital US occurrences annually. The recommended treatment is a strong electrical shock, to reset the cardiac electrical activity, and allow resumption of a normal heart beat. The imperfect understanding of defibrillation mechanisms and the high dimensionality of its parameter space are obstacles to optimization of defibrillation treatment protocols. This work focuses on virtual electrodes, which are charges occurring at cardiac boundaries, (e. g. cardiac and blood vessel surfaces), due to shock induced alterations in the transmembrane potential. They are of primary importance for defibrillation. We present evidence that a dynamically growing wave front, starting at the heart surface, and aided by the dynamics of the fibrillation scroll waves to be more important than small, isolated blood vessels in terminating fibrillation. This conclusion is important for multiple reasons. It sheds light on mechanisms of virtual electrode formation and defibrillation. It allows a prioritization of experimental, simulation and modeling focus, It places more emphasis on larger experimental animals for assessing novel low strength defibrillation strategies.

I. OVERVIEW

A. Background

Ventricular fibrillation is a common cause of cardiac arrest. It is a fatal condition in the absence of prompt treatment. In both normal and fibrillatory states, the electrical dynamics are organized in moving wave fronts in the voltage difference between the interior of the cardiac cells and the extracellular medium (i.e., the transmembrane potential). In a normal heart, the moving electrical wave front proceeds from bottom to top and induces the contractions that pump the blood, whereas in a fibrillatory state, the moving wave fronts are chaotic, and organized into rotating scroll waves, with a centerline, the filament. Treatment for fibrillation is generally through an electrical shock, giving rise to modifications in the transmembrane potential, called virtual electrodes¹ (VE), at cardiac surfaces (including

blood vessels) where the electrical conductivity is discontinuous. The VE disrupt the scroll waves which sustain fibrillation, and possibly their organizing centers, the filaments, in accomplishing defibrillation.

Shock treatment protocol parameters include the electrode location and the intensity, duration, and orientation of the electric field; their optimization is an ongoing research effort. We focus on the details of shock-induced virtual electrode formation (not on defibrillation per se) and thus consider only a portion of the high dimensional optimization problem. We do not complete the full time frame of multiple low energy shocks. In fact for the initial conditions and shock strength selected, chosen to emphasize the importance of small blood vessels, we find that virtually the entire heart is depolarized after a single shock episode, so that there is no basis to continue to later shocks. An important defibrillating mechanism is the development of propagating wave fronts, starting at the VE and initiated at the onset of the shock (make waves) or its termination (break waves). Strong and weak shocks obey distinct defibrillation mechanisms, with the strong shock defibrillation resulting from break front waves, which leave most of the cardiac tissue in a non excitable state². The blood vessels play a supporting role². A complementary approach, known as Low Energy Antifibrillation Pacing (LEAP) uses multiple weak shocks; our primary focus is the weak shock.

B. Main Results

A variety of causal factors (which are not mutually exclusive) have been proposed to explain defibrillation. We performed simulations incorporating novel implementation algorithms using a variety of geometrical meshes (including the whole heart) to study the role of the boundaries of the heart tissue at the wall surfaces and blood vessels. Our main results provide evidence that small vessels play only a minor role in the defibrillation process, while virtual electrodes formed at the heart surface play a primary role by generating large wave fronts that impinge on the existing fibrillatory scroll waves. We also study the sensitivity of post-shock activity on model parameters such as vessel wall conductivity, wall thickness, and tissue conductivity. Other than these sensitivity studies all simulations use a common model of cardiac electrical properties.

C. Purported mechanisms of defibrillation

The causal factors proposed for defibrillation, are: (a) distributed sources, (b) filament-wall interaction, (c) filament tension, (d) stochastically dynamic filament motion, (e) the growing depolarized region (wave front) and (f) the global geometry and dimension (size) of the cardiac tissue. These have been identified under various names in the literature. They are partially overlapping, i.e., non exclusive. The distributed source hypothesis (a) states that a large number of distributed weaker sources of VE act to extinguish filaments and lead to the success of LEAP³. Virtual electrodes may be associated with electrical discontinuities located at the boundaries of fatty tissue within the heart or intra cellular clefts, and with diseased tissue⁴⁻⁶, in addition to those associated with blood vessel walls and the heart walls. The filament-wall hypothesis (b) states that virtual electrodes disrupt the surfaces to which the filaments are attached, thus fundamentally altering scroll wave dynamics which are driven by filament shape (and filaments must end on no-flux boundaries or be closed curves (i.e., scroll rings)⁷. The filament tension hypothesis (c) states that tissue properties themselves can determine filament stability⁸. If the heart substrate supports filaments with positive tension then unanchored filaments tend to shrink and thus self-terminate. However, if the tissue properties lead to negative filament tension then unanchored filaments expand and multiply, in which case defibrillation is much more difficult because the shock must terminate all pre-shock scroll waves. The stochastically dynamic filament motion hypothesis states that the probabilistic nature of defibrillation results from the location of filaments at the time of the shock and from a post-shock random motion of the filaments. (Filament motion during fibrillation tends to be very dynamic⁹.) The growing depolarized region hypothesis (e) states that virtual electrodes generate growing wave fronts and that the growing region behind these wave fronts is unable to sustain a filament. The shape and size of the heart (f) hypothesis states that the large boundary areas at the boundaries of the heart surfaces (e.g., blood in the chamber cavities and inside surface of the heart) play a dominant role in defibrillation because of the large contiguous virtual electrodes created at these boundaries. Moreover, it states that volume to surface ratio or linear dimension of the heart plays a role, and it states that as the electrical currents seek a minimum resistance pathway, the global surface geometry and the fiber orientation are important. In our questioning of a dominant role for causal factor (a), distributed sources, we choose

simulation protocols (initial conditions and shock voltages) which are maximally favorable to this causal factor.

D. Small Blood Vessels

An analytically based study³ supports the distributed sources hypothesis, with conclusions linked to LEAP experimental outcomes through a theory-experimental match in the time required to terminate fibrillation. On the outer (epicardial) surface of the heart, their generation of a growing wave front observed there, and the eventual coalescence of the region behind the wave fronts on the epicardial surface provide the experimental evidence in support of this hypothesis.

There are two questions which we raise regarding this analysis. First, the blood vessels (large and small) are densely and well distributed on the epicardial surface of the heart, but especially those of significant size appear to be sparse and isolated within the cardiac interior tissue. In the rabbit, shown in a cross sectional slice throughout the paper, larger vessels are all located on or near the outer heart surface where they tend to cluster. The remaining blood vessels are isolated, for example in the septum between the two ventricle chambers. In the rat, Figs. 1, and 4, where we lack the heart geometry data, the blood vessels also appear to cluster on the outer cardiac surface.

The rat model has a highly resolved vasculature with only a single branch (veins or arteries, not both), many fine scale blood vessels and no cardiac surface. The 3D defibrillation weak shock in the rat is distinctly less successful than that for the rabbit. In contrast, the rabbit has both blood vessels and a cardiac surface. The rabbit small blood vessels have little effect. Blood vessels below 50 microns in radius are missing from the rabbit data. We conclude that the small blood vessels (rat) are distinctly less important than the cardiac surface (rabbit) in this simulation. Examination of the time developed rabbit 3D defibrillation shock simulations (with and without blood vessel walls) shows that small blood vessels play no role in the dynamics. The wave front simply sweeps through the small blood vessels (where isolated, and they often are) with no enhancement of the wave front by the blood vessel.

The theoretical analysis of ref.³ includes (as we also document) a minimum radius for a blood vessel to participate in the formation of a VE. In their analysis, this radius is

proportional to $1/E$ where E is the applied electrical field strength. For the largest of the shock voltages, 3 V/cm, considered in ref.³, we find a minimum blood vessel size of 200 - 400 microns outer radius. For this size and especially for the size $10\times$ larger, resulting from the weakest of the shocks considered, $10\times$ weaker, the blood vessels cannot be considered to be well distributed.

A second question concerns the minimum radius for a blood vessel to participate in a make wave. This minimum radius is computed approximately in ref.³. The approximate value is sufficient to determine scaling law exponents, which are used in an asymptotic analysis. Quantitative limitations of these estimates result from the omission of the blood vessel wall conductivity, the approximations introduced into the cardiac equations, with a single conductivity replacing the four separate ones of the bidomain model, and with no allowance for the orientation of the fibers relative to the electric field gradient, as they wrap around the blood vessel. Quantitative changes in this minimum blood vessel radius by factors of 2 or 4 appear to result from these omitted factors. Changes in the minimum radius have a significant effect on the density and well distributed nature of the remaining, larger radius, blood vessels observed in the data cited here.

We examine the Bishop et al.² characterization of the 200 micron minimum blood vessel radius for participation in a break wave initiation. Depending on the fiber orientation, we find agreement with this value for the case of arteries or an increase in the minimum radius. With veins and depending on the fiber orientation, increases in the minimum radius are possible according to our slab geometry studies. Some details of the test are modified in this comparison. Our tests are for make waves, for 3D simulations of the full ventricle and for highly resolved slab simulations.

The exceptional nature of the epicardial surface could play a role in the experimental observations of the distributed sources. The dense and well distributed nature of the blood vessels and the gradual coalescence of the make wave excited regions starting at distributed sources under a LEAP regime are observed experimentally³ on the epicardial surface. The bulk of the epicardial surface is a generator of VE, a fact which assists the epicardial surface small blood vessels in initiating make waves.

In view of the two questions raised with the small blood vessel analysis, we believe its extrapolation from the epicardial surface to the cardiac interior should be revisited. Improved resolution anatomical models with resolution 25 microns cf. Fig. 1c¹¹, including

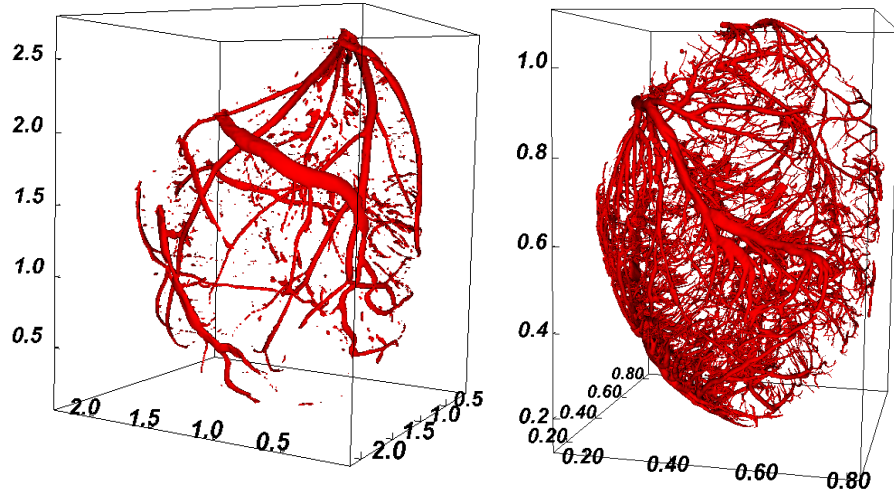


FIG. 1. Sharply contrasting levels of detail in the experimental resolution of cardiac vasculature (units in cm). Left: rabbit, right: rat (scale for rat dimensions estimated from data in ref.¹⁰).

identification of separate arterial and venous systems without gaps, so that each forms a single connected network, would allow identification of fine scale modeling features. 3D simulations based on this data, using physiological parameters for blood vessel wall thickness and conductivity and fiber orientation could then assess whether the small scale blood vessels provide only a contributory and helping role or a leading and central role in the generation of growing make/break regions to cover a sufficient volume to neutralize any scroll waves. Ref.² follows this program for a quasi-two-dimensional thickened slice cut from the rabbit heart. Revisiting could include examination of alternate hypotheses, such as the possibility that distributed VE sources on the VE epicardial surface function as postulated, while the propagation of the resulting make wave into the interior is essentially self sustained, with only minor assistance from the blood vessels.

These suggestions for further research reflect limitations of the current study, in the area of input biological data and in the completeness of the analysis of the small blood vessels relative to the many aspects of the LEAP protocols, with its multiple repeated shocks, its range of applied shock strengths, its range of initial conditions for the ionic currents and the influence of electrode placement. Here we consider only the strongest of the proposed LEAP shocks and ionic state initial conditions most favorable to the generation of make waves.

The refs.¹²⁻¹⁴ develop causal models and protocols for defibrillation. The first two of these references concern strong defibrillating shocks and is largely disjoint from the emphasis of

this paper, with a focus on tunneling of a wave front through windows of excitability within the fibrillating state. The third reference concerns weak shocks and multiple defibrillating shocks in the spirit of³. This reference describes a 3D simulation study of the right ventricle, with major blood vessels included. The origin of the major VE signals are found in the high curvature regions of the cardiac surface, with large blood vessels located on the epicardial surface contributing. These findings and choice of methodology support our major conclusions, that the small blood vessels do not matter and that the global geometry of the cardiac surface and the fiber orientation are more important. It also supports in silica the experimental study³ of feasible low energy weak but repeated shocks in a defibrillation protocol. This reference is mainly concerned with the design and optimization of treatment protocols and does not address causal factors in the sense discussed in this paper.

E. Other Defibrillating Causal Factors

Our simulations of the 3D rabbit model show a growing wave front moving across the heart. This is the growing depolarized region hypothesis, see Sec. III B, and in the absence of distributed sources. The wave fronts must grow to a sufficient volume to force defibrillation.

The motion of the scroll waves and filaments, a part of two of the LEAP hypothesized causal factors, is discussed in ref.². Motion of the scroll waves over the period of the LEAP wave train is documented in Fig. 1e top row of ref.³, in the supplementary materials for ref.⁹ and in the present study.

We show that filament-VE interactions over the LEAP time scale allow a defibrillation contribution from the statistically dynamic motion of the filaments. The physical dimensions of the heart then become a significant variable, in that the interior points of meandering filaments have a diminished chance of meeting a heart chamber surface as the chamber wall becomes thicker, quantified by a dimensional analysis presented here. The statistically dynamic filament hypothesis also deals with circular filaments, having no point of contact with heart boundaries or large blood vessels.

The physical dimension of the heart appears to be a highly significant variable. In the absence of distributed sources, the other defibrillation mechanisms involve a distance (for influence to propagate). Cardiac dimensions have been emphasized through an analysis of the minimum dimensions to sustain a scroll wave¹⁵, and are known medically as a heart

disease risk factor.

The filament-wall interaction hypothesis assumes that the outer regions of a scroll wave interact with depolarized tissue and thereby alter the filament dynamics. A simulation study⁷ finds delayed scroll wave termination, after a few scroll wave rotations, with scroll waves interacting with VE at the epicardial and endocardial surfaces, in support of this hypothesis.

The filament tension hypothesis is based on the observation that a filament will be dynamically unstable and will contract once its end point on a heart chamber wall or large blood vessel has been severed due to a VE induced depolarized region, Modeling and simulation studies^{16,17} support this hypothesis, with the terminology of unpinning. Once unpinned, the unstable filament end can only repin to a heart surface wall or to a large blood vessel of outer radius at least $w/2$, where w is the electrical wave front width¹⁸. The value of $w \sim 500$ microns was determined⁹, leading to minimum repinning radius of 250 microns, rather close to the minimum VE radius of 200 to 400 microns estimated here and in the literature. The same analysis applies to the pinning of filaments in the first place, so that only larger blood vessels can play this role.

II. METHODS

A. Equations of Electro Physiology

The standard bidomain equations for cardiac electro physiology¹⁹ consist of a diffusion equation for the voltages (in the intra cellular and extracellular cardiac tissue and non cardiac tissue called bath) coupled to an ordinary differential equation for the ionic currents. The extracellular voltage and the bath voltage are solved as a single continuous potential, with no flux (Neumann) boundary conditions for the external bath boundary and a discontinuous diffusion tensor across the heart-bath boundary.

The solution domain is denoted by $\Omega = \mathbb{H} \cup \mathbb{B}$, where \mathbb{H} is the heart tissue and \mathbb{B} is the bath. The boundaries of the heart tissue and bath are denoted by $\partial\mathbb{H}$ and $\partial\mathbb{B}$ respectively. The governing bidomain equations with the boundary conditions can be written as²⁰

$$\chi(C_m \frac{\partial v}{\partial e} + I_{ion}(v, w)) - \nabla \cdot (D_i \nabla v) - \nabla \cdot (D_e \nabla v_e) = 0, \quad in \mathbb{H} \quad (1)$$

$$\nabla \cdot (D_i \nabla v) + \nabla \cdot ((D_i + D_e) \nabla v_e) = 0, \quad \text{in } \mathbb{H} \quad (2)$$

$$\frac{\partial w}{\partial t} + g(v, w) = 0, \quad \text{in } \mathbb{H} \quad (3)$$

$$\nabla \cdot (D_b \nabla v_e) = 0, \quad \text{in } \mathbb{B} \quad (4)$$

$$\mathbf{n} \cdot (D_i \nabla v) + \mathbf{n} \cdot (D_i \nabla v_e) = 0, \quad \text{on } \partial \mathbb{H} \quad (5)$$

$$\mathbf{n} \cdot (D_e \nabla v_e) = \mathbf{n} \cdot (D_b \nabla v_e), \quad \text{on } \partial \mathbb{H} \quad (6)$$

$$\mathbf{n} \cdot (D_e \nabla v_e) = I_e, \quad \text{on } \partial \mathbb{B} \setminus \partial \mathbb{H} \quad (7)$$

where χ is the surface to volume ratio of the membrane, C_m is the electrical capacitance of the cardiac tissue per unit area, I_{ion} is the ionic current over the membrane per unit area, which is calculated by the transmembrane potential v and the gate variable w . The gate function g and I_{ion} are determined by the cell ionic model, including the electroporation current²¹⁻²³ I_{ep} . The intra cellular and extracellular potentials and intra and extra conductivity tensors, denoted by v_i , v_e , D_i and D_e respectively, are defined in the heart tissue \mathbb{H} . The extracellular potential is also defined in the bath \mathbb{B} with the bath conductivity D_b . The unit normal vector at the cardiac surface, \mathbf{n} , is oriented outward while I_e represents the electrical current across $\partial \mathbb{B} \setminus \partial \mathbb{H}$.

B. Numerical Methods and Parameters

Our simulation platform is the Chaste (Cancer, Heart and Soft Tissue Environment) software^{19,24,25}, a finite element code for the diffusion of the electrical potentials, and the Rudy model LR1²⁶ for the ionic currents, augmented with an electroporation current, and further augmented (LR-A²⁷) for enhanced numerical stability, a feature needed for modeling of electroporation. The finite element code is supported by a mesh adapted to the boundary of the cardiac tissue.

The rabbit model²⁸, used here and in ref.², is taken from the Chaste web site. The raw data has a resolution of $45 \times 43 \times 36$ microns¹¹, so that analysis of structures finer than 100 microns is problematic. An algorithm, apparently new, constructs outer blood vessel walls from a given inner wall, see supplementary materials item 6* of the methods section. In the present study, the algorithm was applied to the construction of the outer arterial wall only.

The finite element mesh has a total of about 42M elements. The mesh is not uniform, with larger mesh elements in the bath. Within the cardiac tissue, the average of tetrahedron

edge length is 124 microns. For the heart surface triangles, including blood vessel walls, the average edge length is 114 microns.

Blood vessels as small as 50 microns in radius are resolved in this mesh. The visualization mesh (blood vessels only) of Fig. 1, right, is identical to the simulation mesh.

The time step used for the diffusion equation is 0.01 ms. This choice was tested for time step refinement in 1D and 3D studies (details not shown), with identical results. The time step for the ionic currents is set by an adaptive ODE solver, to ensure convergence of the simulation. Fine ionic current time steps are needed during voltage shock transients.

The rat mesh, constructed here, has 48M tetrahedrons, an average edge length of 64 microns and an average edge length of surface triangle of 32 microns. Blood vessels as small as 15 microns in radius are resolved. No blood vessel walls are included.

If a human heart, two times larger in lateral dimensions than a rabbit heart, were simulated, the number of mesh elements increases by a factor of 8, to about 500M elements.

Computational times, with a good preconditioner for the diffusion matrix, increase by a similar factor. A conclusion of this analysis, coupled with the view that the cardiac dimensions are a key input to defibrillation studies, is that scientifically meaningful approximations and simplifications of the computational model will be essential for future progress.

We consider two defibrillating voltages, a typical traditional defibrillation shock of 50 V/cm²¹, denoted here as a strong shock, and 3 V/cm shock, the strongest of those considered in ref.³, denoted here as a weak shock. The transmembrane initial conditions for all simulations are set at -83 mV. for all spatial locations. The shock voltage is imposed at the left and right edges of the bath, in the orientation as shown in the 2D slices, with the positive electrode on the left.

Additional simulation issues are discussed in the Supplementary Materials.

C. Physiological Parameters

Cardiac tissue, blood vessel wall and bath conductivities are given in Table I, and except as explicitly noted in the text, from lines 1 and 2 of Table I. Alternate conductivity values appear in the literature, see Table II. Alternate values for blood conductivity of 0.7 S/m and blood vessel wall conductivity of 0.17 S/m have been reported²⁹.

The blood vessel wall thickness $l = 3.87a^{0.63}$ depends on the vessel outer radius a , with l

TABLE I. Conductivity in S/m of various regions of the rabbit heart. The isotropic intra cellular and extracellular conductivities are calculated as the harmonic mean³².

Tissue type	longitudinal	transverse	Reference
intra cellular	0.174	0.0192	2
extracellular	0.625	0.236	2
	isotropic		
intra cellular	harmonic mean 0.017		32
extracellular	harmonic mean 0.173		32
vessel wall	0.01		11,33
blood	1.0		11,33
bath	1.0		11

TABLE II. Experimental and rabbit simulation cardiac conductivity as used by various authors. I: intra cellular; E: extracellular L: longitudinal; T: transverse ; B: bath, all values in S/m. Ref.² states: [The values used] “were then uniformly scaled to reduce conduction velocity by 25%, in-line with similar reductions shown during heart failure”.

Reference	IL	IT	EL	ET	B
	Experiment				
Clerc ³⁴	0.17	0.019	0.62	0.34	
Roberts el al. ³⁵	0.28	0.026	0.22	0.13	
Roberts et al. ³⁶	0.34	0.060	0.12	0.080	
	Simulation				
Bishop et al. ²	0.174	0.0193	0.625	0.236	1.0
Bishop et al. ³⁷	0.34	0.060	0.12	0.080	1.0

and a in microns^{11,30}, as discussed in Sec. III F 2 and in the Supplementary Materials. This formula is appropriate for arteries and the larger arterioles, It is applicable to the rabbit vessels when considered as arteries. For smaller arteries in slab geometry studies, the values of ref.³¹ will be used. For veins, the wall thickness is $0.09a$, following ref.³¹.

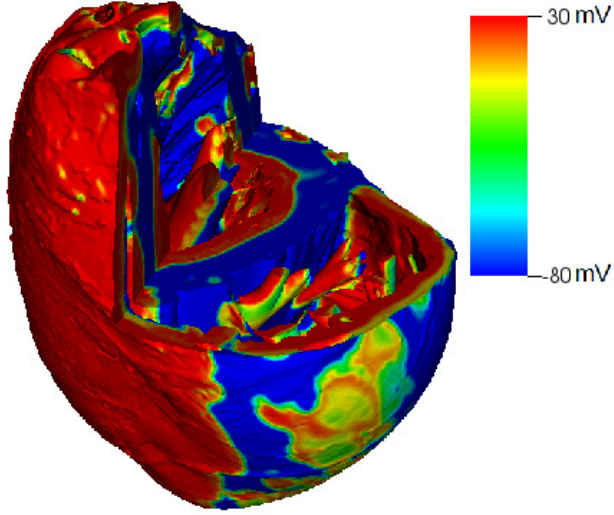


FIG. 2. Simulation of transmembrane voltage at 4 ms after initiation of a weak shock. The blood vessel wall conductivity is 0.01 S/m.

III. RESULTS

A. Visualization of 3D solutions

In Fig. 2, we show the transmembrane voltage on the cardiac surface, with a cut-away showing an interior slice and portions of the interior surface. The image shown is taken after 4 ms of onset of a weak shock, with blood vessel wall conductivity 0.01 S/m. The main features of this simulation and variations on it are examined in the following sections.

B. Small Blood Vessels and VE

1. *Rabbit-Rat comparisons*

In Fig. 3, we show slices of the rabbit (left) and rat (right) transmembrane voltages at 1 ms. This figure shows the concentration of blood vessels on the epicardial surface.

In Fig. 4, we assess the (lack of) importance of the small blood vessels for the rat model. The rat model has small scale blood vessels and no heart surface. The comparison allows a detailed analysis of the relative roles of the cardiac surface (missing) and the small blood vessels (well resolved) based directly on the experimentally observed vascular geometry. We show a strong shock defibrillation, indicating the robustness of the strong shock defibrillation,

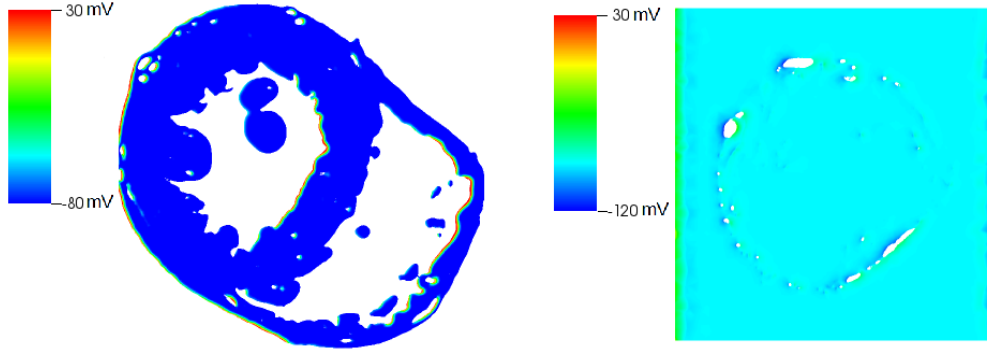


FIG. 3. A slice through the rabbit (left) and rat (right) models, at 1 ms after application of a weak shock. The white regions within the heart are the blood vessels, evidentially concentrated on the epicardial surface.

which appears to succeed (in so far as evaluated here) in the absence of either small blood vessels (rabbit) or of the heart chamber surfaces (rat). The response from the weak shock shows a much smaller depolarized region after shock termination for the rat, in the absence of the heart chamber surface (rat), than for the absence of the small blood vessels (rabbit). On this basis, we conclude that the cardiac walls (rabbit) are more important for defibrillation than are the small blood vessels (rat). The rat simulation is isotropic, as the rat heart geometry is not published, so that fibers, the heart surface and anisotropic modeling are omitted. To allow a uniform comparison, the rabbit simulation is here repeated in an isotropic mode as well, shown in the lower frames.

The surface transmembrane fronts observed in the upper frame of Fig. 4 arise from the direct contact of cardiac tissue with the electrodes (no bath is included in the rat model). They are seen evolving in a symmetric manner near the two edges of the domain. A sequence of smaller time steps is shown in the Supplementary Material.

The effect of the isotropic as opposed to anisotropic simulation can be assessed through comparison to Fig. 8. The isotropic simulation shows a modest decrease in the depolarized region.

C. Dynamic wave fronts

The major claim of this paper is that within the rabbit model, a single weak defibrillation shock achieves its primary effect through a moving wave front, starting at the VE

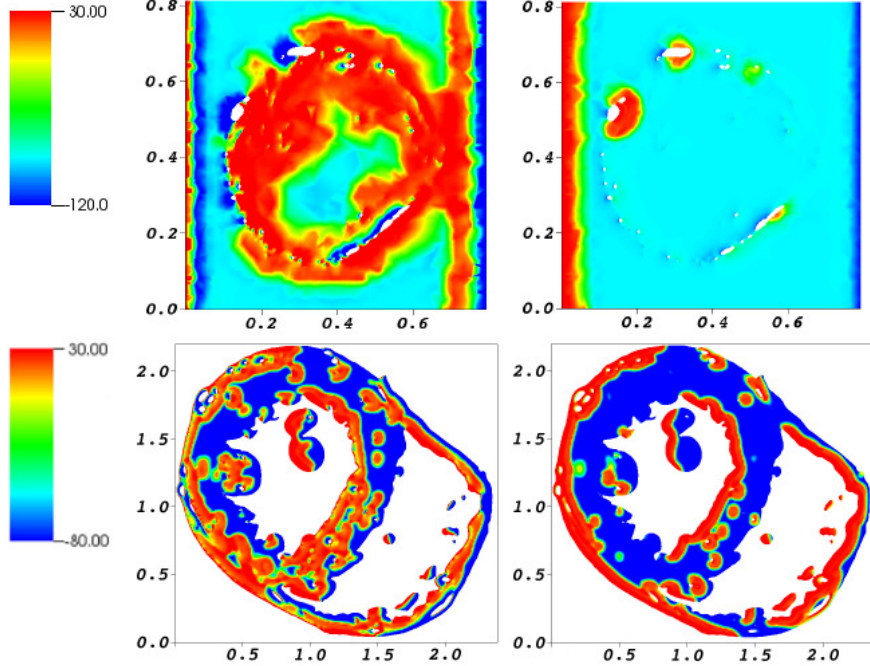


FIG. 4. The transmembrane voltage at 4 ms after shock initiation is shown in color contour plots for strong and weak (left and right frames) shocks in 2D slices from 3D simulations, units in cm, blood vessel walls with no thickness. Above: rat, vasculature only. Below: rabbit, isotropic simulation, included for assessment of isotropic model on simulation results.

located at the cardiac surfaces, primarily the epicardial surface. In this, it is aided by VE associated with the larger blood vessels but not primarily driven by them and receives little or no enhancement from the smaller blood vessels. To achieve success, the region swept by the moving wave front does not need to encompass the entire heart, but only a sufficient fraction of the heart so that other mechanisms discussed here can contribute to terminate the fibrillation state. In Fig. 5 we show 4 frames, as a sequence of time steps ($t = 1, 4, 7, 10$ ms) in the evolution of the wave front as evidence in support of this claim. Additional time steps are shown in the supplementary materials.

D. Filament dynamics and VE interactions

Filament dynamics may play a defibrillation role especially in cases where the shock strength is lower, for larger animals, or where different initial states are encountered. As a surrogate for this phenomena, we consider the 3 V/cm simulation at 4 ms, at which time

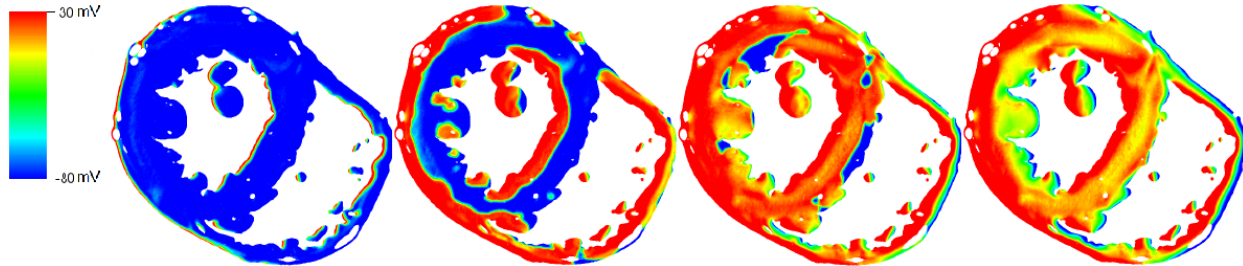


FIG. 5. A color plot of the transmembrane voltage is shown for a slice through the heart front from a 3D simulation of the application of a weak shock. The four frames are for times $t = 1, 4, 7, 10$ ms after the shock initiation. From the sequence, the origin of the moving wave front at the epicardial surface is clear as is its continued growth with larger blood vessels assisting but not primary drivers of the growth.

the depolarized region is about 25% of the cardiac domain. We show in Fig. 6 (multimedia view) three time steps relevant to weak shock dynamics (1700, 1750, 2000 ms), starting at the initial time 1698 ms with data taken from a movie of filament dynamics⁹. The dynamic filaments are initially yellow everywhere and change to blue after the first encounter of a given filament segment or subsegment with any portion of the depolarized region which has grown from the VE. We observe the overlap of filament locations (dynamic) with VE locations (static) to represent the probabilistic nature of defibrillation.

If we consider the meandering motion of the filament as a Brownian motion, then the formula $S(t) = \text{erf}((x_1 - x_0)/2\sqrt{Dt})$ for the Brownian motion probability $S(t)$ of first passage time t from the current position x_0 to a wall location x_1 along a normal line through the cardiac wall becomes relevant. We identify the dimensionless group $(x_1 - x_0)/2\sqrt{Dt}$ to be studied for its relation to defibrillation success. The numerator, $x_1 - x_0$, is related to the wall width and thus to the overall heart dimensions, as relevant to defibrillation. The diffusion coefficient D is the diffusion coefficient of the meandering (lateral) random motion of the filament.

E. Rabbit simulations: the role of global cardiac and fiber geometries

We look for polarized and depolarized regions associated with the blood vessels and for the influence of the blood vessels on the overall dynamics. Any discontinuity or gradient in

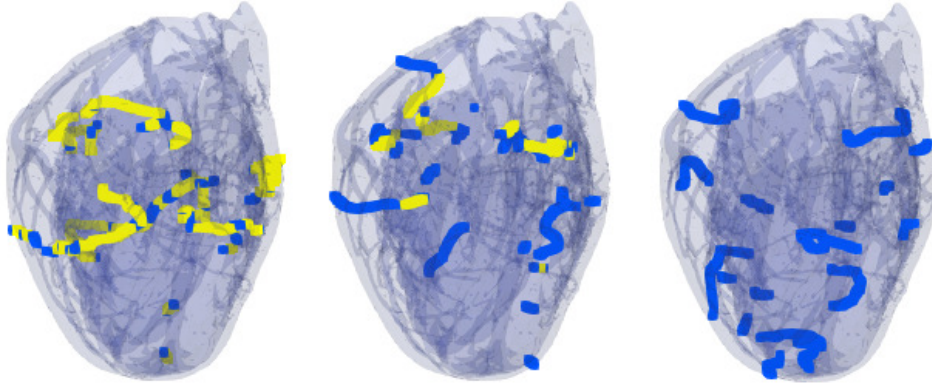


FIG. 6. Three frames based on a reanalysis of previously unpublished filament dynamics for a fibrillation state within the rabbit heart (multimedia view), for times $t = 1700$ (first time step for the dynamics recorded here), 1750, 2000 ms. We thank Pras Pathmanathan for permission to use unpublished filament dynamics simulations by him and one of the authors (RG) as input to our filament dynamics analysis. In the original movie, the fibrillating state in the rabbit was induced by artificially shortening the action potential duration to render the dynamics unstable to fibrillation. The resulting dynamics do not reflect true fibrillation in a rabbit, which could be constrained by the small dimensions of the rabbit heart, but represent a fibrillation state more typical of a larger species. The reanalysis of this movie consists of recording which filament segments reach a VE induced depolarized region (where upon their color is changed from yellow to blue). Thus the filaments segments are all colored yellow at an initial time $t = 1698$ and segments or subsegments are colored blue after an encounter with a VE. We observe the growing dominance of blue as the time evolves.

the conductivities will produce some effect on the transmembrane voltages. Thus, strictly speaking, the notion of a minimum sized blood vessel to produce an effect is not meaningful, or at least depends on some non-zero lower limit on the effect. Furthermore, in the context of 3D simulations we find the effect depends on the global solution structure and not merely on the blood vessel size. Within these caveats, we can find support for the 200 micron minimum radius suggested in ref.². We observe a dependence of the minimum radius on the fiber orientation and vessel type (artery vs. vein).

In Fig. 7, we show details of the growing wave front at 2, 3, and 4 ms of a weak shock

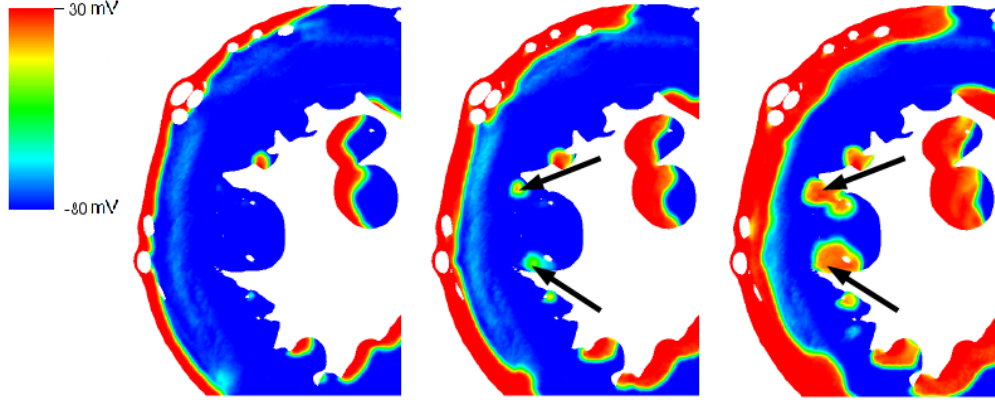


FIG. 7. A VE and make wave origination site caused by a resulting channel of high current flow, enhanced by global features of the fiber orientation. The make wave is near but distinct from a region of high surface curvature and from a small but isolated blood vessel. In this sense the cause of this make wave has to be found in the global geometry of the cardiac surface and of the fiber orientation. The three frames are for times $t = 2, 3, 4$ ms after the shock initiation.

in the rabbit model. At the locations marked by arrows, a developing wave front forms. The location is near but not exactly coincident with a region of high surface curvature. The growing wave front (a VE with no associated cardiac surface) originates in a region of high current flow, and is due to global features of the fiber orientation and associated high conductivity channels, not to local features of surface curvature.

F. Sensitivity studies

Uncertainty or variability regarding multiple model parameters is a common feature of biological modeling. We select for analysis what appear to be the more significant of these: shock strength, vessel wall conductivity and thickness and tissue conductivity.

1. Wall conductivity

In Fig. 8, we show the sensitivity of the transmembrane voltage to the blood vessel wall conductivity, with values of 0.01, 0.20, 1.0 S/m. In effect, the value 1.0 corresponds to the absence of a vessel wall.

From Fig. 8 we see an observable but not major expansion of the depolarized region as

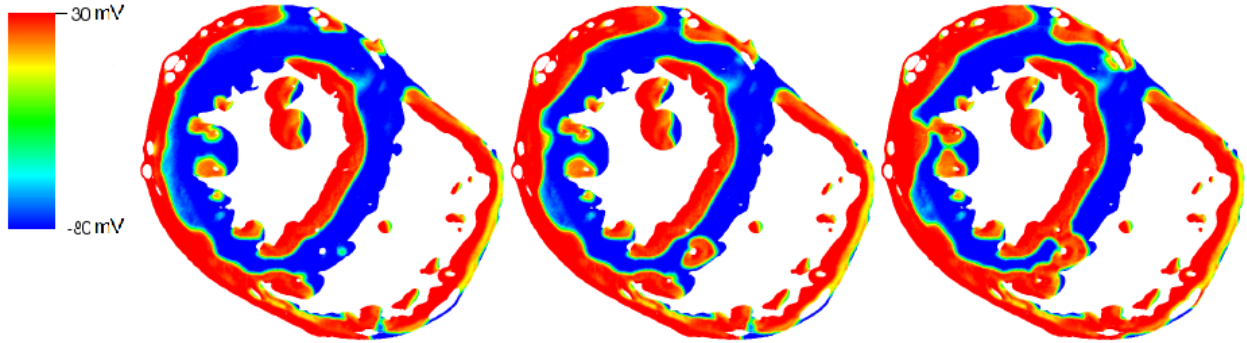


FIG. 8. Transmembrane voltage sensitivity to blood vessel wall conductivity, shown 4 ms after weak shock initiation. Left to right, blood vessel wall conductivities of 0.01, 0.20 and 1.0 S/m. The right frame, with wall conductivity equal to that of blood is equivalent to no wall for the blood vessel.

the vessel wall conductivity is increased. Within the context of the studies of this paper, the wall conductivity of the larger blood vessels perhaps matters, but only at a level of finer detail, while this variable for the smaller blood vessels appears to have no influence.

2. *Blood vessel minimum radius: slab geometry*

In an idealized slab geometry, we employ the identical cell model and conductivities as with the 3D rabbit geometry simulation. Thus only the geometry and the mesh (which is finer for the slab) are modified. We determine the minimum blood vessel outer radius to generate a significant make wave response to a weak defibrillation shock. The response and the minimum blood vessel radius depends strongly on several factors identified here. They depend on the vessel type (a vein or artery to fix its wall thickness as a function of the radius, and including an artificial type with no wall at all) and they depend on the orientation of the fibers relative to the gradient of the applied electrical field. We assume in all cases that the electric field and the fibers are orthogonal to the blood vessel and we assume that the initial state of the tissue in the slab is polarized. With the variables considered, we form Table III whose entries are the minimum radii in each of six cases. Additional documentation to justify the table entries is placed in the supplementary materials.

Thus we consider a long slab, $15000 \times 1600 \times 400$ units in microns, and blood vessels, of outer radius 100, 200 and 400 microns. For each blood vessel radius, we consider three types

TABLE III. Minimum outer radius (microns) of a blood vessel having a significant response to a weak electrical shock for each of six cases based on a wall conductivity of 0.1 S/m. Results of a highly resolved study of an isolated blood vessel in an idealized slab geometry are shown.

	Artery	vein	no wall
fibers perpendicular	200	400	400
fibers parallel	> 400	> 400	400

of blood vessels. Arteries have a wall thickness $l = 3.87a^{0.63}$ as in Sec. II C for 100 micron and larger artery vessels. Veins have a wall thickness of 10% of the inner radius. The vein and small artery wall thickness is from ref.³¹. The third blood vessel type has no wall. The wall conductivity is 0.01 S/m in all cases.

The artery and to a lesser extent, the vein is a resistive element as far as the electrical current is concerned. The low conductivity of the vessel wall is an opposite and stronger effect than the high conductivity of the blood (except in the case of no wall). Current will preferentially flow around and not through the vessel. To see this, consider the extracellular current along the slab center line through the vessel. The resistances (length/conductivity) add, and are greater than the corresponding values through tissue. The same applies to other current streamline passing through the vessel. The result is a net resistive effect for the vessel, until the fiber orientations are included.

The fiber orientation preferentially enhances or counters the flow of current streamlines around the vessel, and thus adds to its resistive nature or counters and possibly reverses this effect. The conductivity is higher in the direction of the fiber. When the fibers are perpendicular to the electric field gradient, the ability to flow around the vessel is enhanced. When the fibers are parallel to the electric field gradient, the ability to flow around the blood vessel is diminished or even reversed.

On this basis, we observe a reversed polarity response for the perpendicular fibers, weakening and then disappearing as the wall becomes thinner (veins and no wall). We see a total effect stronger for the perpendicular than the parallel fibers case. In combination, the low wall conductance and the fiber orientation either combine to give a stronger effect or oppose to give a weaker effect and possibly of a different direction. In the case of no wall, with the

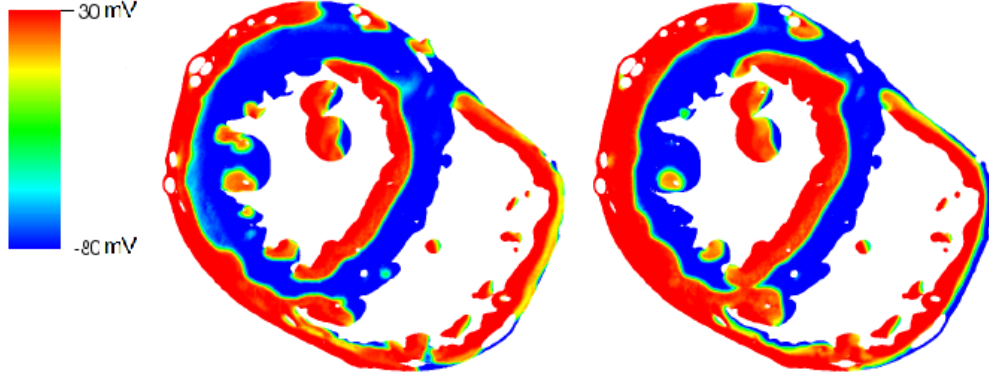


FIG. 9. Transmembrane voltages at 4 ms after a weak shock initiation are shown in a color plots in slices through 3D simulations for a strong shock. The frames follow the order of the lines in Table II, for two sets of conductivity values. The difference between the two frames is not significant.

enhanced conductivity of the blood, the current will preferentially flow through the blood vessel. Here the case of perpendicular fibers enhances this effect, while the case of parallel fibers diminishes the effect.

These combinations of effects lead to the 6 different entries in Table III and in the detailed effects observed in the Supplementary Materials. In summary, we see a minimum radius for all but two cases, with the value for the minimum radius depending on the fiber orientation and the blood vessel type.

3. *Cardiac tissue conductance*

In Fig. 9, we compare transmembrane voltages for distinct cardiac conductivity matrices at 4 ms after a weak shock initiation, showing slices through 3D simulations, frames in the order of Table II. We find differences in detail at intermediate times, but an overall qualitative and semiquantitative agreement between the solutions based on the different conductivities.

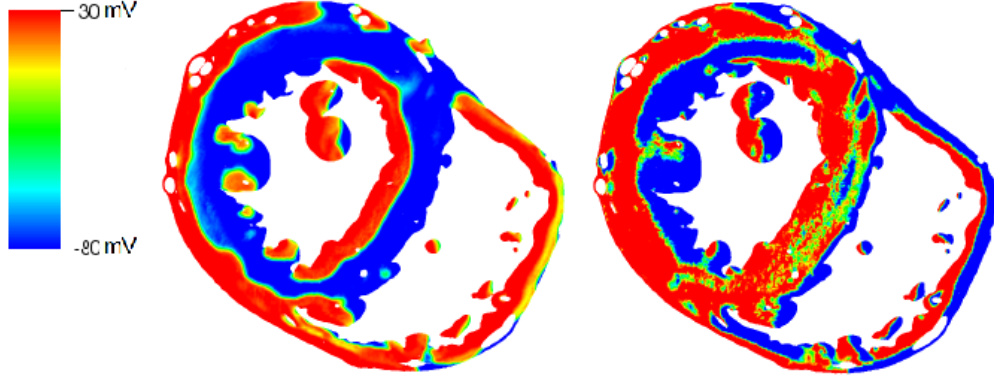


FIG. 10. Transmembrane voltages show a strong sensitivity to shock strength, in slices through 3D simulations of a rabbit, shown 4 ms after shock initiation. Blood vessel wall conductivity 0.01 S/m. Left: weak shock, 3 V/cm. Right, strong shock, 50 V/cm.

4. *Shock voltage*

The dynamics for the strong and the weak shocks are very different, with the strong shock setting up polarized and depolarized channels between the epicardial and endocardial surfaces where these ionic states are originally induced as VE. The weak shock allows for a stronger influence of the fiber direction diffusion, dominantly parallel to the endocardial and epicardial surfaces. For this case, the polarized regions grow in a regular fashion, starting at the epicardial and endocardial surfaces where they first arise from the cardiac surface VE.

The strong sensitivity to shock voltage is shown in Fig. 10.

IV. CONCLUSIONS

The main conclusion of our simulations of the rabbit model is that a growing wave front, starting at the epicardial surface, aided but not driven by the large blood vessels, and aided by the dynamic motion of the filaments is the primary effect of a weak defibrillation shock. We find that the large scale aspects of the cardiac surface and the larger blood vessels are more important than the smaller blood vessel walls in the generation of VE. Blood vessels 100 microns in radius or smaller do not contribute appreciably to the rabbit weak shock simulations.

We cite six partially overlapping causal factors for the interaction of filaments with VE, leading to weak shock defibrillation. The first postulate, of widely distributed VE, is di-

minished in our simulations as a driver of the defibrillation make wave. The second and third hypotheses involve the dynamics of filaments, either meandering statistically or with a motion influenced by the partially neutralized scroll waves. Our results show the viability of the dynamically meandering hypothesis. The fourth postulate is the filament tension hypothesis, of self annihilation of a filament with “cut off” ends. The main conclusion of the paper is to support the fifth hypothesis, of dynamically moving wave fronts starting at the epicardial surface. The cardiac size is the sixth causal factor. The heart size is of paramount importance for defibrillation success. Larger hearts tend to support more complex dynamics including more filaments, thus making defibrillation more difficult. Size here should be considered in the context of the cell model dynamics. We note the observation of ref.⁹ that the rabbit is closer to a human in its cardiac and fibrillation properties than many other animals. For the rabbit and human, fibrillation is postulated to be quasi-two-dimensional, where as, for example in a dog, the fibrillation state could be remarkably different and fully 3D. The cardiac size is a driver of computational efforts, and leads to excessive requirements, especially for the repeated simulations needed for scientific progress, and for studies of the human heart. Thus, the importance of scientifically justified approximations and simplifications in the simulation modeling is evident.

A sensitivity study of the VE to the blood vessel wall conductivity, wall thickness, clustering vs. localized blood vessels and mesh refinement was also presented.

V. SUPPLEMENTARY MATERIAL

We propose eight software developments to be used in conjunction with electro cardiac packages, including an algorithm which appears to be new for the construction of outer walls of blood vessels from a given inner wall. See supplementary material (URL link). We present complete time sequences for the six simulations of Fig. 8 and also the time sequence 1 to 4 ms for the rat simulation, strong and weak shocks of Fig. 4. We show details of the slab geometry study to justify conclusions regarding minimum radii for VE effectiveness.

ACKNOWLEDGMENTS

The authors would like to thank the development team of the Chaste software, especially Martin Bishop (King's College London) and Pras Pathmanathan (FDA), for the use of the software package and the rabbit heart mesh. We thank the authors of ref.³² for sharing a prepublication copy of their work. We also thank Pras Pathmanathan for permission to use unpublished filament dynamics simulations by him and one of the authors (RG) as input to our filament dynamics analysis. This research was supported in part by the NSF grant NSF CPS-1446832. Results in this paper were obtained using the high-performance LIRed computing system at the Institute for Advanced Computational Science at Stony Brook University.

REFERENCES

- ¹E. A. Sobie, R. C. Susil, and L. Tung, *Biophysical Journal* **73**, 1410 (1997).
- ²M. J. Bishop, G. Plank, and E. Vigmond, *Circulation: Arrhythmia and Electrophysiology* **5**, 210 (2012).
- ³S. Luther, F. H. Fenton, B. G. Kornreich, A. Squires, P. Bittihn, D. Hornung, and M. Z. et al, *Nature* **475**, 235 (2011).
- ⁴F. H. Fenton, S. Luther, E. M. Cherry, N. F. Otani, V. Krinsky, A. Pumir, E. Bodenschatz, and R. F. Gilmour, *Circulation* **120**, 467 (2009).
- ⁵R. Plonsey, *Biophysical Journal* **39**, 309 (1982).
- ⁶V. G. Fast, S. Rohr, A. M. Gillis, and A. G. Klber, *Circ. Res.* **82**, 375 (1998).
- ⁷C. Zemlin, S. Mironov, and A. Pertsov, *J Cardiovasc Electrophysiol.* **14**, S257 (2003).
- ⁸V. N. Biktashev, A. V. Holden, and H. Zhang, *Phil. Trans. R. Soc. A* **347**, 611 (1994).
- ⁹P. Pathmanathan and R. A. Gray, *BioMed Research International* **2015**, 14 pages (2015).
- ¹⁰H. C. Ott, T. S. Matthiesen, S.-K. Goh, L. D. Black, S. M. Kren, T. I. Netoff, and D. A. Taylor, *Nature Medicine* **14**, 213 (2008).
- ¹¹M. Bishop, P. M. Boyle, G. Plank, D. G. Walsh, and E. Vigmond, *IEEE Transactions on Biomedical Engineering* **10**, 2335 (2010).
- ¹²T. Ashihara, J. Constantino, and N. Trayanova, *Circ. Res.* **102**, 737 (2008).
- ¹³J. Constantino, Y. Long, T. Ashihara, and N. Trayanova, *Heart Rhythm* **7**, 953 (2010).

- ¹⁴L. J. Rantner, B. M. Tice, and N. A. Trayanova, *Heart Rhythm* **10** (2013).
- ¹⁵D. Blendea, R. Dadu, and C. A. McPherson, *InTech* (2013).
- ¹⁶S. Takagi, A. Pumir, D. Paz, I. Efimov, V. Nikolski, and V. Krinsky, *Phys. Rev. Lett.* **93**, 058101 (2004).
- ¹⁷A. Pumir, V. Nikolski, M. Horning, A. Isomura, K. Agladze, K. Yoshikawa, R. Gilmour, E. Bodenschatz, and V. Krinsky, *Phys. Rev. Lett.* **99**, 208101 (2007).
- ¹⁸A. M. Pertsov, in *Discontinuous propagation in the heart*, edited by P. M. Spooner and J. Jalife (Future, 1997).
- ¹⁹G. R. Mirams, C. J. Arthurs, M. O. Bernabeu, and et al., *PLoS Computational Biology* **9**, e1002970 (2013).
- ²⁰S. Xue, H. Lim, J. Glimm, F. H. Fenton, and E. M. Cherry, *SISC* **38**, B100 (2016), Stony Brook University Preprint SUNYSB-AMS-15-03.
- ²¹W. Krassowska, *Pacing and Clinical Electrophysiology* **18**, 1644 (1995).
- ²²D. K. Cheng, L. Tung, and E. A. Sobie, *American Journal of Physiology - Heart and Circulatory Physiology* **277**, H351 (1999).
- ²³T. Ashihara and N. A. Trayanova, *Biophysical Journal* **87**, 2271 (2004).
- ²⁴P. Pathmanathan and R. A. Gray, *Int. J. Numer. Methods Biomed. Eng.* **30**, 525 (2014).
- ²⁵P. Pathmanathan, M. Bernabeu, R. Bordas, J. Cooper, A. Garny, J. Pitt-Francis, J. Whiteley, and D. Gavaghan, *Prog. Biophys. Mol. Biol.* **102**, 136 (2010).
- ²⁶C. Luo and Y. Rudy, *Circ Res.* **68**, 1501 (1991).
- ²⁷T. Ashihara and T. Y. et al., *Journal of Cardiovascular Electrophysiology* **12**, 1393 (2001).
- ²⁸M. J. Bishop, G. Plank, R. A. B. Burton, J. E. Schneider, D. J. Gavaghan, and P. K. Vicente Grau, *American Journal of Physiology - Heart and Circulatory Physiology* **298**, H699 (2010).
- ²⁹A. Goldberg, B. B. ans B. Uygun, and M. Y. et al., *Nature* (2015).
- ³⁰B. K. Podesser, F. Neumann, M. Neumann, W. Schreiner, G. Wollenek, and R. Mallinger, *Acta Anatomica: Cells, Tissues, Organs* **163**, 63 (1998).
- ³¹A. C. Burton, *Physiol Rev.* **34**, 619 (1954).
- ³²A. Connolly, E. Vigmond, and M. Bishop, *PLoS One* **12**, e0173324 (2017).
- ³³K. R. Visser, *Proceedings of the Annual Conference of the IEEE Engineering* **5**, 1540 (1989).
- ³⁴L. Clerc, *The Journal of Physiology* **255**, 335 (1976).

³⁵D. E. Roberts, L. T. Hersh, and A. M. Scher, IEEE Trans. Biomedical Eng. **440**, 701 (1982).

³⁶D. E. Roberts, L. T. Hersh, and A. M. Scher, Cir. Res. **50**, 342 (1982).

³⁷M. Bishop and G. Plank, Biomedical Engineering **58**, 1066 (2011).